

1  
2  
3 **Periodic Dispersion-Corrected Approach for Isolation Spectroscopy of N<sub>2</sub>**  
4  
5 **in an Argon Environment: Clusters, Surfaces and Matrices**  
6  
7

8 Y. Makina,<sup>a)</sup> K. Mahjoubi,<sup>a)</sup> D. M. Benoit,<sup>b),\*</sup> N.-E. Jaidane,<sup>a)</sup> M. Mogren Al-Mogren,<sup>c)</sup> and M.  
9 Hochlaf<sup>d),\*</sup>  
10

11  
12  
13 <sup>a)</sup> Laboratoire de Spectroscopie Atomique, Moléculaire et Applications – LSAMA, Université de  
14 Tunis El Manar, Tunis, Tunisie.

15 <sup>b)</sup> Department of Chemistry, University of Hull, HU6 7RX, UK.

16  
17 <sup>c)</sup> Chemistry Department, Faculty of Science, King Saud University, PO Box 2455, Riyadh 11451,  
18 Kingdom of Saudi Arabia  
19

20 <sup>d)</sup> Université Paris-Est, Laboratoire Modélisation et Simulation Multi Echelle, MSME UMR 8208  
21 CNRS, 5 bd Descartes, 77454 Marne-la-Vallée, France  
22  
23  
24

25 This document is the Accepted Manuscript version of a Published Work that appeared in final form in  
26 Journal of Physical Chemistry A, copyright © American Chemical Society after peer review and technical editing by the publisher.  
27 To access the final edited and published work see <https://pubs.acs.org/doi/10.1021/acs.jpca.7b00093>.  
28  
29  
30  
31  
32  
33  
34  
35  
36

37 

---

  
38 <sup>\*)</sup> Corresponding authors:  
39

40 D. M. Benoit: [D.Benoit@hull.ac.uk](mailto:D.Benoit@hull.ac.uk)

41 M. Hochlaf: [hochlaf@univ-mlv.fr](mailto:hochlaf@univ-mlv.fr)  
42  
43  
44  
45  
46  
47  
48  
49  
50  
51  
52  
53  
54  
55  
56  
57  
58  
59  
60

**ABSTRACT**

*ab initio* and PBE density functional theory with dispersion correction (PBE-D3) calculations are performed to study  $N_2-Ar_n$  ( $n \leq 3$ ) complexes and  $N_2$  trapped in Ar matrix (*i.e.*  $N_2@Ar$ ). For cluster computations, we used both Møller-Plesset (MP2) and PBE-D3 methods. For  $N_2@Ar$ , we used a periodic-dispersion corrected model for Ar matrix, which consists on a slab of four layers of Ar atoms. We determined the equilibrium structures and binding energies of  $N_2$  interacting with these entities. We also deduced the  $N_2$  vibrational frequency shifts caused by clustering or embedding compared to an isolated  $N_2$  molecule. Upon complexation or embedding, the vibrational frequency of  $N_2$  is slightly shifted whilst its equilibrium distance remains unchanged. This is due to the weak interactions between  $N_2$  and Ar within these compounds. Our calculations show the importance of inclusion of dispersion effects for the accurate description of geometrical and spectroscopic parameters of  $N_2$  either isolated, in interaction with Ar surfaces or trapped in Ar matrices.

## I. INTRODUCTION

The study of interactions between rare-gas atoms and molecules provides a wealth of information on molecular properties (matrix spectroscopies, for example) but also on how their properties are modified by their environments (i.e. matrix shift) [1]. It has been shown that if the interaction between the rare-gas atoms and the molecule is weak, the molecular properties are only slightly perturbed by the surrounding environment and thus are a very close to those of the isolated molecule [2]. This condition is satisfied for neutral van der Waals (vdW) complexes containing molecules interacting with rare gas atoms [3]. Such interactions play important roles in several chemical, physical and biological media [3-8]. They are in subtle balance with electrostatic (ES) and exchange-repulsion (ER) interactions. For instance, they control the 3D structures of DNA and proteins, crystal packing, aggregates formation, and the orientation of molecules when approaching surfaces [9,10].

Several theoretical and experimental studies have been devoted to probing the spectroscopy of di- and poly-atomic molecules interacting with either rare-gas atoms or rare-gas matrices. These include, for instance, CO, NO, Cl<sub>2</sub>, CO<sub>2</sub>, C<sub>3</sub>, O<sub>3</sub> and NO<sub>2</sub> molecules [4-8] interacting with Ne, Ar, Kr or Xe. A full understanding of the effects occurring at the atomic scale requires reliable and relevant information on the potential energy surfaces of these systems. However, obtaining reliable interaction potentials remains challenging due to the many-body nature of those systems.

High accuracy wave-function methods such as the coupled-cluster methods (for example CCSD(T) at the complete basis set (CBS) limit) provide an excellent account of the dispersion energy. However, these methods still suffer from unfavorable computational scaling [ $O(N^7)$ ] leading to large computation times even for medium-sized systems. Density functional theory (DFT), on the other hand, has an intrinsically lower computational cost, but standard approaches do not describe dispersion interactions accurately. To try to correct this drawback, various DFT techniques have been proposed to improve the description of dispersion interactions in the theory. Those are, for example, the non-local van der Waals density functional (vdW-DF) [11,12], the DFT symmetry-adapted perturbation theory (DFT-SAPT) [13,14] including more rigorous partitioning of intermolecular energies, the density functional theory/coupled cluster method (DFT/CC) based on the pairwise representability of the difference between the CCSD(T) and DFT energies [15], the density functional (DF) that takes into account the dispersion interaction from a physical point of view [16], and the empirically-corrected DFT-D approach [17-20]. Over the years, the DFT-D approach has been widely used because of its simplicity, low computational overhead and reliability.

The present contribution examines the case of an N<sub>2</sub> molecule interacting with small Ar clusters, surfaces or embedded into an Ar matrix. Because of its importance for atmospheric and planetary processes [21,22], the Ar-N<sub>2</sub> cluster has been widely studied both theoretically [23-35] and experimentally [36-39]. These studies have provided an accurate characterization of this complex, of its potential energy surface and of its vibrational and rotational spectra. In particular, they established

1  
2  
3 the existence of two minima of Ar–N<sub>2</sub>: a linear structure and a T-shaped structure, located in shallow  
4 potential wells (a few tens of cm<sup>-1</sup>). Note that large and medium-sized mixed Ar<sub>n</sub>-N<sub>2m</sub> clusters (n >  
5 200) have also been widely investigated [40-46] whereas we are not aware of studies of small N<sub>2</sub>-Ar<sub>n</sub>  
6 clusters (1 ≤ n ≤ 5). In the case of methane clusters, for example, Sanaa Zaag et al. [47] showed that  
7 small clusters may behave differently and possess different properties and reactivities than medium-  
8 sized or large clusters. Hence small N<sub>2</sub>-Ar<sub>n</sub> clusters deserve specific investigations, which is one of the  
9 aims of this study.

10  
11  
12  
13  
14 The present computations were carried out using the same first-principles methodology for all  
15 environments (gas phase clusters, molecules adsorbed on a rare-gas surface or embedded into a rare-  
16 gas matrix). We compute the equilibrium structures and interaction potentials thus enabling us to  
17 examine the vibrational and structural effects caused by clustering or embedding. This highlights the  
18 induced environment effects on the structure and the spectroscopy of N<sub>2</sub>. Moreover, we establish the  
19 efficiency of the DFT-D3 method in accounting for the anisotropy of the interaction at the molecular  
20 level for all types of environments studied.

21  
22  
23  
24 Our paper is arranged as follows: we briefly describe the computational details in Section II.  
25 Our results for N<sub>2</sub>-Ar<sub>n</sub> clusters are presented in Section III. Section IV contains the data relative to N<sub>2</sub>  
26 adsorbed on Ar surfaces or embedded in an Ar matrix. We discuss our findings in Section V.  
27  
28  
29

## 30 II. COMPUTATIONAL METHODS

31  
32 The DFT-D approach considers dispersion as an additive, pairwise, energy correction term,  
33 C<sub>6</sub>R<sup>-6</sup>, where R and C<sub>6</sub> are the interatomic distances and the dispersion coefficients, respectively  
34 [19,48,49]. Various versions of DFT-D have been proposed. The latest iteration proposed by Grimme  
35 *et al.* [13,18] includes third-order dispersion corrections and removes some of the initial empiricism  
36 (DFT-D3). Moreover, Grimme and co-workers introduced geometry-dependent information to  
37 improve transferability that was lacking in DFT-D1 [19] and DFT-D2 [20]. Several benchmark studies  
38 showed that DFT-D3 results differ from those obtained with CCSD(T) by less than 5-10%  
39 [17,18,50,51]. In addition, this approach has been shown to provide a reliable description of rare-gas  
40 interactions, which are usually hard to describe using uncorrected DFT functionals [52].

41  
42  
43  
44 In this study, we use the Gaussian plane waves (GPW) method [53-57] to account for the  
45 periodicity of the embedded system. This approach uses pseudopotential associated Gaussian basis  
46 sets for the expansion of the Kohn-Sham valence orbitals, and auxiliary plane waves basis set for the  
47 description of the electronic density as implemented in the Quickstep code [56,58,59], which is a part  
48 of the CP2K open source program [60]. The interaction of valence electrons with the nuclei is  
49 modeled by means of relativistic, norm-conserving, separable, dual-space Gaussian-type  
50 pseudopotentials of Goedecker, Teter, and Hutter (GTH) [61], optimized for the gradient-corrected  
51 exchange-correlation functional of Perdew, Burke, and Ernzerhof (PBE) [62]. This functional is used  
52 for all our calculations following a careful benchmarking in our previous study [52].  
53  
54  
55  
56  
57  
58  
59  
60

1  
2  
3 For molecular systems, a cut-off energy  $E_{\text{cut}} = 400$  Ry was found to be sufficient. The atomic  
4 geometry of the matrix models, surfaces, molecules and dimers are optimized by minimizing the  
5 energy using the BFGS optimizer [63]. The convergence criteria between the current and the last  
6 optimizer iteration are: the maximum geometry change is set to  $5 \times 10^{-4}$  bohr, the root mean square  
7 (RMS) geometry change is set to  $2.5 \times 10^{-4}$  bohr and the maximum force component of the current  
8 configuration is set to  $10^{-6}$  bohr $^{-1} \times$  Hartree.

9  
10 To model the  $\text{N}_2\text{-Ar}_n$  cluster systems, we use a supercell of  $20 \times 20 \times 20$  Å in size. We  
11 remove the periodic images and use a 0-D analytic Poisson solver for the electrostatic terms. We use  
12 the QZV3P-GTH basis set [53,64] for Ar atoms and the diffuse aug-QZV3P-GTH basis set [53,64] for  
13 N atoms (the exponents of all polarization functions are taken from Dunning's aug-cc-pVXZ (X = T,  
14 Q) basis sets [16,65]). The  $\text{N}_2\text{-Ar}_n$  (n = 1, 2, 3) clusters are computed using Moller-Plesset second-  
15 order perturbation theory (MP2) [65–67] in conjunction with Dunning and co-worker's aug-cc-pVXZ  
16 (X= T, Q) basis sets as implemented in Gaussian 09 package [68]. Additional CCSD(T) calculations  
17 are performed using the CFOUR suite of programs (V1.0) [69].

18  
19 For each system, the DFT-D3 total energy is computed as the sum of the conventional DFT  
20 energy and the correction value based on a damped atom-pairwise potential [17]. The counterpoise  
21 correction for the basis set superposition error (BSSE) [70] was not considered during the DFT-D3  
22 calculation for our large systems (adsorbed molecule and embedded into Ar matrices), as suggested by  
23 Grimme [17,18] but was used for all wave-function based cluster calculations.

### 24 25 26 27 28 29 30 31 32 33 III. $\text{N}_2\text{-Ar}_n$ (n = 0, 1, 2, 3) CLUSTERS

#### 34 35 a) The Isolated Nitrogen Molecule

36 We start our investigations by a series of test calculations for the isolated  $\text{N}_2$  molecule to  
37 benchmark our theoretical approach, the basis sets and the pseudopotentials. We compute the  
38 equilibrium distance and the vibrational frequency of isolated  $\text{N}_2$  in its electronic ground state ( $X^1\Sigma_g^+$ )  
39 using CCSD(T) and MP2 post Hartree–Fock methods in conjunction with the aug-cc-pVXZ (X= T, Q)  
40 basis sets. We also use the dispersion-corrected Density Functional Theory using the PBE functional  
41 with the GTH pseudopotential and aug-TZV2P or aug-QZV3P basis sets. Our results and their  
42 comparison to experimental data are listed in Table 1.  
43  
44  
45  
46  
47  
48  
49  
50  
51  
52  
53  
54  
55  
56  
57  
58  
59  
60

**Table 1: Equilibrium Distance ( $r_e$ , Å) and Harmonic Vibrational Frequency ( $\omega_e$ ,  $\text{cm}^{-1}$ ) of  $\text{N}_2$  ( $X^1\Sigma_g^+$ ) Computed Using Various Methods and Basis Sets. The Notation FC Indicates Frozen-Core CCSD(T) Calculations. Deviations From the Experimental Results are Given in Square Brackets. Note that the Given Experimental Vibrational Frequency is the Harmonic Value. The Experimental Fundamental Frequency for  $\text{N}_2$  is  $\tilde{\nu} = 2329.9 \text{ cm}^{-1}$  [71].**

Method	Basis set	$r_e$	$\omega_e$
MP2	aug-cc-pVTZ	1.114 [0.016]	2186.8 [-171.8]
	aug-cc-pVQZ	1.110 [0.012]	2201.6 [-157.0]
PBE-D3	aug-TZV2P-GTH	1.102 [0.004]	2350.9 [-7.7]
	aug-QZV3P-GTH	1.102 [0.004]	2344.8 [-13.8]
CCSD(T)	aug-cc-pVTZ(FC)	1.104 [0.006]	2340.0 [-18.6]
	aug-cc-pVQZ(FC)	1.101 [0.003]	2354.5 [-4.1]
Experiment <sup>a)</sup>	---	1.098	2358.6

a) Ref. [71].

Table 1 shows that MP2 provides the least satisfactory description of both distances and frequencies, with deviations of the order of  $\sim 0.01 \text{ Å}$  and  $\sim 171 \text{ cm}^{-1}$ , respectively. As expected, CCSD(T) leads to an order of magnitude improvement for both quantities, with largest deviations of the order of  $\sim 0.006 \text{ Å}$  and  $\sim 20 \text{ cm}^{-1}$  and will be considered as computational reference for our study. Interestingly, both PBE-D3/aug-TZV2P and PBE-D3/aug-QZV3P-GTH give the same distance (1.102 Å) which is similar to that obtained with CCSD(T). For the harmonic vibrational frequency, MP2/aug-cc-pVXZ (X= T, Q) levels underestimate  $\omega_e$  in comparison to experiment (deviations of more than  $170 \text{ cm}^{-1}$ ) whereas CCSD(T) and PBE-D3 reassuringly agree well with the experimental value (differences of few  $\text{cm}^{-1}$  for the largest basis sets). The correlation effects present in the N–N system are poorly described by MP2, which is to be expected. However, PBE-D3 combined with either aug-TZV2P-GTH or aug-QZV3P-GTH basis sets performs as well as CCSD(T)/aug-cc-VQZ. This is particularly interesting given the much lower computational cost of PBE-D3 as compared to CCSD(T). Therefore, PBE-D3/aug-QZV3P-GTH constitutes a cost-effective method of choice for the description of  $\text{N}_2$  in various environments.

### b) The $\text{N}_2$ –Ar Cluster

The  $\text{N}_2$ –Ar complex is a typical system that displays van der Waals interactions. It is characterized by the dominance of pure dispersion interactions. As mentioned in the introduction, two minimum energy structures exist for the  $\text{N}_2$ –Ar cluster: a T-shaped form and a linear form. The geometrical parameters and harmonic vibrational frequencies of these two stable geometries are listed in Table 2.

**Table 2: Harmonic Frequencies ( $\omega_i$ ,  $\text{cm}^{-1}$ ) and Equilibrium Geometries of T-shaped and Linear Structures of  $\text{N}_2\text{-Ar}$  Complex.  $r_e$ ,  $R$  and  $\theta$  are the Jacobi Coordinates (Figure 1). Distances are in  $\text{\AA}$  and Angles are in Degrees.  $\omega_1$  is the Harmonic Vibrational Frequency of  $\text{N}_2$ . The Vibrational Shift From the Free  $\text{N}_2$  Frequency is Shown in square Brackets. BE (meV) is the Binding Energy of the Complex.**

Linear form			
Method	MP2 <sup>a)</sup>	PBE-D3 <sup>b)</sup>	CCSD(T) <sup>c)</sup>
$r_e$	1.11	1.10	1.10
$R$	4.72	4.37	4.20
$\theta$	0.0	0.0	0.0
BE	-8.9	-13.4	-9.7 (Ref [14])
$\omega_1$	2185.4 [+1.4]	2344.9 [-0.2]	2339.3 [+0.7]
$\omega_2$	36.9	217.4	35.1
$\omega_3$	6.0	191.1	12.6
T-shaped form			
Method	MP2 <sup>a)</sup>	PBE-D3 <sup>b)</sup>	CCSD(T) <sup>c)</sup>
$r_e$	1.11	1.10	1.10
$R$	3.63	3.75	3.68
$\theta$	90.0	89.8	90.0
BE	-11.2	-17.3	-12.4 (Ref [14])
$\omega_1$	2185.3 [+1.5]	2344.9 [-0.2]	2339.5 [-0.5]
$\omega_2$	41.4	231.7	36.4
$\omega_3$	12.3	177.0	6.1

a) aug-cc-pVTZ basis set

b) aug-QZV3P-GTH and QZV3P-GTH basis sets for N and Ar.

c) aug-cc-pVTZ basis set.

Table 2 shows that our computed equilibrium parameters  $R$  and  $\theta$  (as defined in Figure 1 below) are in satisfactory agreement with the high-level CCSD(T) calculations. Indeed, the  $R$  distance is 4.37  $\text{\AA}$  for PBE-D3 and 4.20  $\text{\AA}$  at the CCSD(T) level for the linear form of  $\text{N}_2\text{-Ar}$  and  $R = 3.75$   $\text{\AA}$  and  $R = 3.68$   $\text{\AA}$  using PBE-D3 and CCSD(T) for the T-shaped form, whereas MP2 provides an  $R$  distance that deviates noticeably from CCSD(T) for the linear form. As was the case above for isolated  $\text{N}_2$ , MP2 underestimates the N–N stretch, while PBE-D3 is remarkably close to CCSD(T). Overall, the magnitude of the vibrational shift is small ( $\sim 1.5$   $\text{cm}^{-1}$  for MP2,  $\sim 0$   $\text{cm}^{-1}$  for PBE-D3 and  $\sim 0.5$   $\text{cm}^{-1}$  for CCSD(T)) and remains similar for both configurations at all levels of theory.

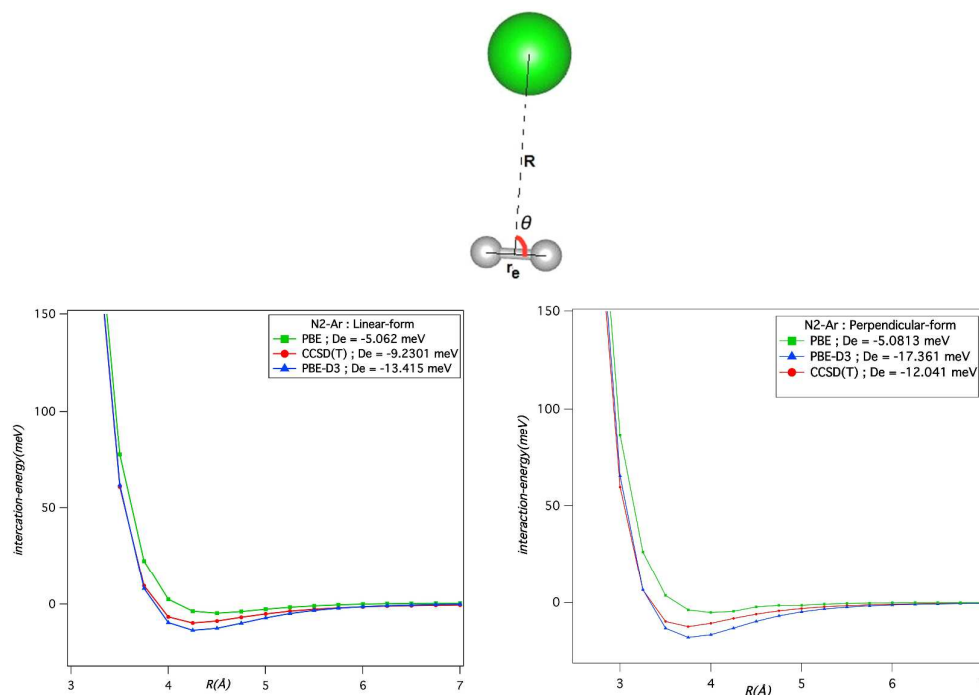


**Figure 1:** Upper panel: Definition of the  $r_e$ ,  $R$  and  $\theta$  parameters. Lower panel: Potential energy for T-shaped and linear forms of  $N_2$ -Ar obtained with PBE DFT with and without dispersion correction D3, where Ar is described using the QZV3P basis set and N by the aug-QZV3P-GTH basis set. We also show the potential calculated at the CCSD(T)/aug-cc-pVTZ+BF level [24].

Figure 1 displays one-dimensional cuts of the 3D potential energy surface (3D-PES) of  $N_2$ -Ar along the  $R$  Jacobi coordinate for perpendicular ( $\theta = 90^\circ$ , T-shape form) and collinear ( $\theta = 0^\circ$ , linear form) configuration. These potentials are computed using the PBE-D3 method with and without dispersion correction (i.e. standard PBE) and compared to the CCSD(T) calculations of Ref [24]. This enables us to assess the performance of the corrected dispersion density functional method for this van der Waals complex. For these cuts, the N-N distance ( $r_e$ ) is fixed at  $1.10 \text{ \AA}$ .

Figure 1 shows that PBE, PBE-D3 and CCSD(T) potentials present minima, corresponding to the T-shaped and linear  $N_2$ -Ar clusters. Nevertheless, the depth of these potential wells depends on the method used for computations. Indeed, we compute a binding energy (BE) of the T-shaped form of  $-5.1 \text{ meV}$ ,  $-17.3 \text{ meV}$  and  $-12.0 \text{ meV}$  using PBE, PBE-D3 and CCSD(T), respectively. For the linear form, BE is evaluated  $-5.1 \text{ meV}$ ,  $-13.4 \text{ meV}$ ,  $-9.2 \text{ meV}$  at the PBE, PBE-D3 and CCSD(T) levels. Our results indicate clearly that including the dispersion correction D3 is crucial for the description of the potential energy with DFT since it leads to deeper potentials, in agreement with the CCSD(T) results. Hence, D3 dispersion correction improves the characterization of the energy profile of these vdW systems. Nevertheless, it seems that PBE-D3 overestimates the dispersion energy as the well depths



are overestimated for both forms. Our results on this cluster indicate clearly that we can use a dispersion-corrected density functional level of theory to compute weak non-bonded interactions.

### c) The $N_2$ - $Ar_2$ System

For the  $N_2$ - $Ar_2$  complex, we limited our geometry optimizations to the global minimum which corresponds to a structure where both argon atoms are close to each other. This structure is displayed in Figure 2 and described in Table 3, with a summary of its geometrical parameters and harmonic vibrational frequencies. Note that the minimum energy structure is similar to the most stable form of the  $CO$ - $Ar_2$  system (denoted as Minimum 1 in Ref. [52]).

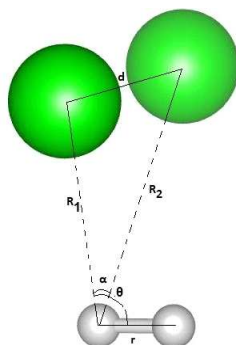


**Figure 2:** The optimized structure of  $N_2$ - $Ar_2$  system. We give also the definition of the geometrical parameters listed in Table 3.

The binding energy of the complex (BE) is computed as the energy difference between the cluster and that of a free  $N_2$  molecule and an  $Ar_2$  dimer. Using MP2, the BE is computed to be  $-26.7$  meV which is smaller than the value obtained using PBE-D3 ( $-33.5$  meV).

**Table 3: Harmonic Frequencies ( $\omega_i$ ,  $cm^{-1}$ ) and Geometrical Parameters of the  $N_2$ - $Ar_2$  Structure at Equilibrium Computed Using MP2/aug-cc-pVTZ and PBE-D3/aug-TZV2P (N)/QZV3P (Ar) Methods. Distances are in Å and Angles are in degrees.  $\omega_1$  is the Harmonic Vibrational Frequency of  $N_2$ . The Vibrational Shift From the Free  $N_2$  Frequency is Shown in Square Brackets. BE (meV) is the Binding Energy of the Complex Computed as the Energy Difference Between the Cluster and that of a Free  $N_2$  Molecule and an  $Ar_2$  Dimer.**

Parameters	MP2	PBE-D3
r	1.11	1.10
$R_1$	3.65	3.86
$R_2$	3.65	3.86
D	3.76	3.81

$\theta$	79.8	80.0
$\alpha$	61.9	61.0
$\omega_1$	2183.8 [+3]	2343.5 [+1.3]
$\omega_2$	47.7	205.1
$\omega_3$	35.8	203.0
$\omega_4$	29.9	186.1
$\omega_5$	13.5	142.0
$\omega_6$	11.3	29.0
BE	-26.7	-33.5

Table 3 also shows that the N–N distance remains almost unchanged upon clustering whereas the harmonic vibrational frequency of N<sub>2</sub> decreases by 1.3 cm<sup>-1</sup> using PBE-D3 method (but by 3 cm<sup>-1</sup> at MP2 level) with respect to that of isolated N<sub>2</sub> molecule. Therefore, there is a negligible effect of complexation on the N–N distance, whereas the N<sub>2</sub> harmonic vibrational frequency is affected. We note that, compared to the CO–Ar<sub>2</sub> complex [52], the inter-monomer distances (R<sub>1</sub>, R<sub>2</sub>) are longer for N<sub>2</sub>–Ar<sub>2</sub>. This is due to the slightly weaker interaction between N<sub>2</sub> and Ar<sub>2</sub> as compared to that of CO and Ar since N<sub>2</sub> is non-polar.

#### d) The N<sub>2</sub>–Ar<sub>3</sub> System

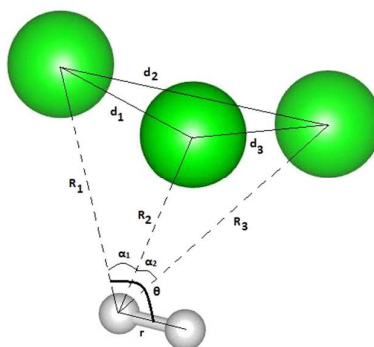


**Figure 3:** Optimized structure of N<sub>2</sub>–Ar<sub>3</sub> system and definition of the parameters listed in Table 4.

Figure 3 presents the most stable form of the N<sub>2</sub>–Ar<sub>3</sub> cluster, which is obtained after several geometry optimizations with different starting structures. This stable structure is formed by a quasi-equilateral triangle constructed by the three Ar atoms situated above the N<sub>2</sub> molecule. The binding energy of this cluster, computed as the energy difference between the cluster and that of a free N<sub>2</sub>

molecule and that of an Ar<sub>3</sub> trimer, is –39.6 meV at the MP2 level and –46.2 meV using the PBE-D3 approach.

**Table 4: Harmonic Frequencies ( $\omega_i$ , cm<sup>-1</sup>) and Geometrical Parameters of N<sub>2</sub>-Ar<sub>3</sub> Structure Using MP2/aug-cc-pVTZ and PBE-D3/aug-TZV2P (N)/QZV3P (Ar) Methods. Distances are in Å and Angles in degrees.  $\omega_1$  is the Harmonic Vibrational Frequency of N<sub>2</sub>. The Vibrational Shift From the Free N<sub>2</sub> Frequency is Shown in Square Brackets. BE (meV) is the Binding Energy of the Cluster, Computed as the Energy Difference Between the Cluster and that of a Free N<sub>2</sub> Molecule and that of an Ar<sub>3</sub> Trimer.**

Parameters	MP2	PBE-D3
R	1.114	1.102
R <sub>1</sub>	3.523	3.725
R <sub>2</sub>	4.137	4.285
R <sub>3</sub>	3.523	3.725
d <sub>1</sub>	3.748	3.930
d <sub>2</sub>	3.759	3.987
d <sub>3</sub>	3.748	3.924
$\theta$	99.36	99.73
$\alpha_1$	57.92	58.2
$\alpha_2$	57.91	58.4
$\omega_1$	2182.1 [+4.7]	2342.9 [+1.9]
$\omega_2$	54.0	208.0
$\omega_3$	51.1	204.9
$\omega_4$	40.3	195.1
$\omega_5$	37.6	148.3
$\omega_6$	27.7	142.5
$\omega_7$	27.7	34.7
$\omega_8$	13.2	24.6
$\omega_9$	8.1	22.8
BE	–39.6	–46.2

Table 4 summarizes the geometrical parameters of this structure. The Ar–N<sub>1</sub>–Ar angles ( $\alpha_i$ ) are similar for both methods, 58°, but there is a difference in the Ar<sub>1</sub>–N<sub>1</sub>–N<sub>2</sub> angle ( $\theta$ ) as seen previously for the N<sub>2</sub>–Ar<sub>2</sub> complex. Also, we notice that the distance between the two nitrogen atoms remains

1  
2  
3 almost unchanged within  $N_2$ -Ar<sub>3</sub> as compared to that of isolated  $N_2$ . As noticed above for  $N_2$ -Ar<sub>2</sub>, the  
4 distances between Ar and N atoms are longer than those computed for CO-Ar<sub>3</sub> [52] because of the  
5 weaker dispersive interaction between  $N_2$  and Ar. Note that the computed harmonic vibrational  
6 frequency shift for  $N_2$  is more noticeable, amounting to  $\sim 2\text{ cm}^{-1}$  using the PBE-D3 method ( $4.7\text{ cm}^{-1}$  at  
7 MP2 level). This is an increase in magnitude compared to  $N_2$ -Ar<sub>2</sub>. Note also that the harmonic  
8 vibrational frequency of  $N_2$  is smaller than that of isolated  $N_2$  ( $X^1\Sigma_g^+$ ).  
9  
10  
11  
12

#### 13 IV. $N_2$ Interacting with Ar Surfaces or Trapped in Ar Matrices

14  
15 In the previous section, we showed that the PBE-D3/aug-QZV3P level of theory gives  
16 accurate enough results, which agree well with CCSD(T) or experimental values for the isolated and  
17 clustered nitrogen molecule. This is associated with a significant reduction of the computational cost  
18 compared to CCSD(T), for example. Thus larger systems, such as  $N_2$  adsorbed on Ar surfaces or  
19 trapped in Ar cold matrices, can be explored with similar accuracy using this approach.  
20  
21  
22  
23

##### 24 a) Pure Ar Crystal

25 We choose to study four layers of 18 Ar atoms as a periodic model for the Ar matrix, which  
26 leads to a cubic unit cell containing 72 Ar atoms. After a PBE-D3/QZV3P optimization of our model  
27 crystal, we calculate a face centered cubic (fcc) lattice of 5.223 Å. This value agrees well with the  
28 experimental value (of 5.222 Å) measured at 0 K by Fujii et al. [72] and with the theoretical value (of  
29 5.30 Å) by Migen Halo *et al.* [73] derived using periodic MP2 computations.  
30  
31  
32  
33

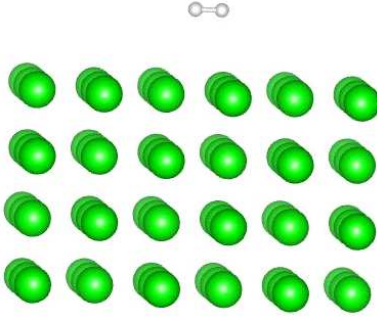
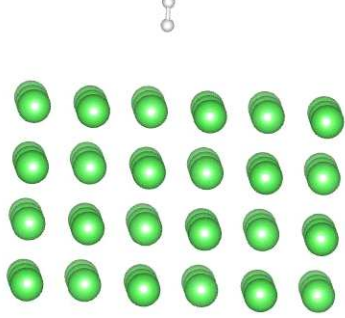
##### 34 b) $N_2$ Interacting with an Ar Surface

35 For these computations, we used our four argon layers model and added  $\sim 20\text{ Å}$  of vacuum  
36 above the surface to construct the super-lattice. The  $N_2$  molecule is then positioned above the Ar  
37 surface. The large size of our super-cell ( $15.669 \times 15.669 \times 25\text{ Å}$ ) minimizes any  $N_2$ - $N_2$  neighboring  
38 periodic interaction. We performed three sets of calculations. We started by fixing all argon atoms,  
39 then, we released the Ar planes one by one by moving away from the molecule. The model where all  
40 Ar layers are fully frozen is denoted as “All 4 layers”. When only the first Ar layer (first two Ar  
41 layers) is relaxed the model is denoted as “Bottom 3 layers” (as “Bottom 2 layers”). Two starting  
42 orientations of the nitrogen molecule were chosen: either perpendicular or parallel to the surface. The  
43 results of these computations are collected in Table 5, where we list the N-N equilibrium distance, its  
44 harmonic frequency and the vibrational shift caused by surface attachment. We also give the binding  
45 energy (BE) of  $N_2$  to the surface computed as the energy difference between the system and that of a  
46 free  $N_2$  molecule and the relaxed argon surface.  
47  
48  
49  
50  
51  
52  
53  
54

55 After optimization, two stable configurations were found:  $N_2$  parallel to the surface and  $N_2$   
56 perpendicular to the surface. Since the electron density on both N atoms is the same, the tilt angle ( $\delta$ )  
57 of the molecular axis of the  $N_2$  molecule with respect to the Ar surface is  $0^\circ$  or  $90^\circ$ . Note that for  
58  
59  
60

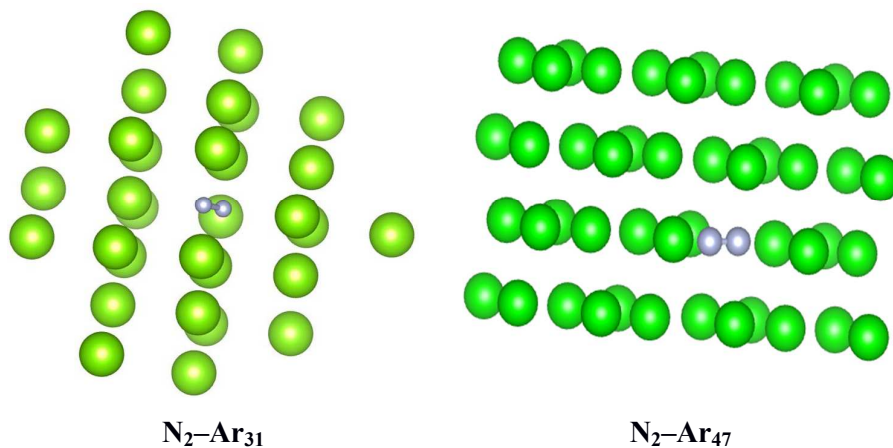
anisotropic electron densities,  $\delta$  is different from these two values. This is the case, for instance, for CO adsorbed on Ar surface [52], or for imidazole and histidine interacting with a gold Au (111) surface [74,75].

**Table 5: Characteristics of the Interaction of N<sub>2</sub> Located Parallel or Perpendicular to an Argon Surface.  $r_e$  (Å) and  $\omega_e$  (cm<sup>-1</sup>) are the N-N Equilibrium Distance and the N<sub>2</sub> Harmonic Vibrational Frequency, respectively.  $\Delta\omega_e$  (cm<sup>-1</sup>) corresponds to the Vibrational Shift with respect to Free N<sub>2</sub>.  $R_e$  (Å) is the Distance from the Centre of Mass of N<sub>2</sub> and the First Ar Layer. BE (meV) is the Binding Energy Surface Computed as the Energy Difference Between the System and that of a Free N<sub>2</sub> Molecule and the Relaxed Argon Surface.**

Number of frozen Ar layers	$r_e$	$\omega_e$	$\Delta\omega_e$	$R_e$	BE
<b>N<sub>2</sub> // Ar<sub>72</sub></b>					
All 4 layers	1.10	2335.3	+9.5	3.74	-42.9
Bottom 3 layers	1.10	2335.0	+9.8	3.71	-45.0
Bottom 2 layers	1.10	2335.0	+9.8	3.79	-45.2
					
<b>N<sub>2</sub> ⊥ Ar<sub>72</sub></b>					
All 4 layers	1.10	2357.2	-12.4	3.69	-25.4
Bottom 3 layers	1.10	2356.9	-12.1	3.66	-28.3
Bottom 2 layers	1.10	2357.3	-12.5	4.02	-28.8
					

1  
2  
3 Table 5 lists the equilibrium geometries of  $N_2$  interacting with the Ar surface models. This  
4 table shows that the N–N equilibrium distance remains unchanged **regardless** of the orientation of the  
5 nitrogen molecule on the argon surface. The distance between  $N_2$  and the Ar surface ( $R_e \sim 3.4 \text{ \AA}$ ) is  
6 relatively long. The computed harmonic frequencies of  $N_2$  are  $2335 \text{ cm}^{-1}$  and  $2357 \text{ cm}^{-1}$  for  $N_2 // Ar_{72}$   
7 and  $N_2 \perp Ar_{72}$  respectively, which correspond to approximate vibrational shifts of  $+10 \text{ cm}^{-1}$  and  $-12$   
8  $\text{cm}^{-1}$  compared to isolated  $N_2$ , respectively. Interestingly, relaxing the Ar layers does not influence the  
9 adsorption **geometry** which is different to what was observed for CO interacting with Ar surface [52].  
10 **Yet the** binding energies of  $N_2$  to the surface **differ** and BE is  $-45.2 \text{ meV}$  for  $N_2 // Ar_{72}$  and  $-28.8 \text{ meV}$   
11 for  $N_2 \perp Ar_{72}$ . **This is consistent with what was observed earlier for the two minimum energy structures**  
12 **of  $N_2$ -Ar (linear and T-shaped) with unchanged N–N distance, but different BEs (stronger binding for**  
13 **the T-shaped structure). Thus, the perpendicular orientation of  $N_2$  on the Ar surface is similar to the**  
14 **linear stationary point of  $N_2$ -Ar and the parallel orientation of  $N_2$  on the Ar surface is similar to the**  
15 **T-shaped stationary point of  $N_2$ -Ar. This is also in agreement with the data obtained for  $N_2$ -Ar<sub>2</sub> and  $N_2$ -**  
16 **Ar<sub>3</sub>. The vibrational shift is strongly dependent on the binding mode with a positive shift for the**  
17 **parallel arrangement and a negative shift for the perpendicular arrangement.**  
18  
19  
20  
21  
22  
23  
24  
25  
26  
27  
28

29 **c)  $N_2$  Molecule Trapped in Argon Matrices**



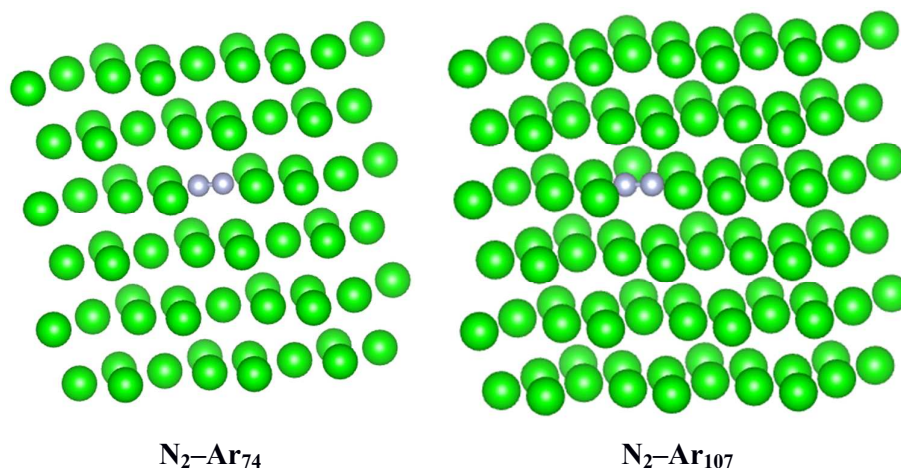


**Figure 4:** Optimized equilibrium structures of  $N_2$  embedded in argon matrices of different sizes.

We treated the nitrogen molecule trapped in argon matrix using PBE-D3 in order to evaluate the effect of the gas rare environment around this diatomic. For that purpose, we used the optimum geometry calculated for pure Ar crystal and we replaced one Ar atom situated in the centre of the unit cell by a  $N_2$  molecule. This procedure ensures that the  $N_2$  molecule is fully embedded in a periodic argon environment. Moreover, we have used four unit cells obtained by translation of the primary unit cell, cell size effects of  $(2 \times 2 \times 2)$ ,  $(3 \times 2 \times 2)$ ,  $(3 \times 3 \times 2)$  and  $(3 \times 3 \times 3)$  were used to assess these effects. These correspond to  $N_2\text{-Ar}_{32}$ ,  $N_2\text{-Ar}_{47}$ ,  $N_2\text{-Ar}_{74}$  and  $N_2\text{-Ar}_{107}$ , where the separation between adjacent nitrogen diatomics increases with the number of Ar atoms in the matrix. Then we performed geometry optimizations. The parameters of the equilibrium structures are depicted in Figure 4 and reported in Table 6.

The experimental vibrational shift is inherently anharmonic as it is computed using the difference between the measured fundamentals for  $N_2@Ar$  (Ref. [76]) and that for a free  $N_2$  molecule (Ref. [71]). In our calculations, we use the computed harmonic frequency of  $N_2$  trapped in argon matrix (Table 6) and the value computed for an isolated  $N_2$  molecule (Table 1) assuming that the anharmonicity constant remains similar in both cases. This approximation allows us to estimate the experimental vibrational shift using only the harmonic approximation.

**Table 6:** Characteristics of  $N_2$  Embedded into Ar Matrices.  $r_e$  (Å) is the Equilibrium Distance of  $N_2$ .  $\omega_e$  ( $\text{cm}^{-1}$ ) is the  $N_2$  Harmonic Vibrational Frequency.  $\Delta\omega_e$  ( $\text{cm}^{-1}$ ) Corresponds to the Vibrational Shift with Respect to Free  $N_2$ .  $R_{NAr}$  (Å) Corresponds to the Distance Between Ar and N and  $R_{N_2-N_2}$  (Å) is the Distance Between  $N_2$  and its Periodic Image.

System	$r_e$	$\omega_e$	$\Delta\omega_e$	$R_{NAr}$	$R_{N_2-N_2}$
free $N_2$	1.103	2344.8	0	–	–
$N_2@Ar_{31}$	1.102	2367.6	-22.8	3.37	10.6
$N_2@Ar_{47}$	1.103	2340.8	+4.0	3.42	12.1

$N_2@Ar_{74}$	1.103	2335.6	+9.2	3.98	14.2
$N_2@Ar_{107}$	1.103	2335.6	+9.2	3.91	15.5
$N_2@Ar_{matrix}$ <sup>a)</sup>	–	2325.9	+4.0	–	–

a) Ref. [76].

Upon embedding, the N–N equilibrium distance ( $r_e$ ) remains almost unchanged. For  $N_2@Ar_{31}$ , the  $N_2$  stretch frequency is computed to be  $2367\text{ cm}^{-1}$  (negative vibrational shift). However, this shift increases as we increase the size of the matrix. Indeed, Table 6 shows that there is a slight decrease in the  $N_2$  harmonic vibrational frequency from  $\sim 2345\text{ cm}^{-1}$  for isolated  $N_2$  to  $2340\text{--}2335\text{ cm}^{-1}$  for  $N_2$  trapped in a matrix made of 47 or 74 or 107 Ar atoms per unit cell. Convergence is reached with an Ar matrix containing at least 74 Ar atoms. The corresponding harmonic vibrational frequency shifts remain then constant at the value of  $\sim 9\text{ cm}^{-1}$ .

Thus,  $N_2$  trapped into a unit cell containing 31 Ar atoms is most likely too small a model to prevent  $N_2$  from interacting with its periodic image. Indeed, the lateral interactions between  $N_2$  and its  $N_2$  image ( $N_2\text{--}N_2$ ) could be the cause for the intermediate harmonic frequency value, as the distance between  $N_2$  and its periodic image is of  $\sim 10.6\text{ \AA}$ . For cells formed by more than 74 Ar the separation between  $N_2$  and its image is larger than  $14.2\text{ \AA}$  and the harmonic  $N_2$  frequency starts converging. In fact, both cells of 31 and 47 Ar atoms are insufficient to completely solvate  $N_2$ . This contrasts with our previous study of CO [52] where the convergence started already with 31 Ar atoms. Since both diatomics have similar sizes, this difference could be related to the different interactions in the  $CO@Ar$  and  $N_2@Ar$  systems, as  $N_2$  is non-polar while CO is polar.

The frequency shift of  $N_2$  trapped in an Ar matrix remains invariant and converges when the nitrogen is fully solvated in the argon matrix ( $Ar_{74}$  matrix). Our theoretical study gives  $\Delta\omega_{N_2} \sim 9\text{ cm}^{-1}$  which is in agreement with the experimental shift ( $\sim 4\text{ cm}^{-1}$  [76]). The remaining deviation can be attributed to anharmonic corrections (which have been assumed to be negligible in this study), possible impurities in the experimental Ar matrix or an overestimation of the weak interactions in the system by the DFT-D3 approach.

## V. DISCUSSION

Our systematic study of the interaction of nitrogen molecule with different environments of argon shows that the presence of argon atoms surrounding the  $N_2$  molecule disturbs its vibrational structure. Indeed, the harmonic vibrational frequency of nitrogen decreases linearly as the number of Ar atoms in the clusters increase until it reaches a plateau for a number of Ar atoms larger than 3. The largest deviation upon clustering or embedding with respect to free  $N_2$  is of  $\sim 9\text{ cm}^{-1}$ . Indeed, the harmonic vibrational frequency of  $N_2$  is nearly unaffected by the presence of a single argon atom. Once we add another Ar atom ( $N_2\text{--}Ar_2$ ,  $N_2\text{--}Ar_3$ ) the vibrational frequency shift increases to  $\sim 2\text{ cm}^{-1}$ . For  $N_2$  interacting with Ar surfaces or embedded in Ar matrices, the shift becomes distinctly larger ( $\sim 9$



1  
2  
3  $\text{cm}^{-1}$ ). In addition, we notice that the vibrational shift of  $\text{N}_2$  interacting with an Ar surface is subject to  
4 strong orientation effects when  $\text{N}_2$  is perpendicular to the Ar surface (negative vibrational shift) or  
5 parallel to the Ar surface (positive vibrational shift).  
6

7 For  $\text{CO-Ar}_n$  [52] and  $\text{HCl-Ar}_n$  ( $n = 1, 2, 3$ ), these effects are slightly larger [77]. Indeed, the  
8 frequency shifts for  $\text{CO-Ar}_n$  are in the range  $\sim 3 \text{ cm}^{-1}$  to  $\sim 8 \text{ cm}^{-1}$  for  $1 \leq n \leq 3$ . This shift equals  
9  $1.76 \text{ cm}^{-1}$  for  $\text{HCl-Ar}$  then becomes  $4.53 \text{ cm}^{-1}$  when  $\text{HCl}$  interacts with three Ar atoms. These  
10 differences may be related to the polarity of the embedded molecule. The gas rare effects on the  
11 harmonic vibrational frequency are in the following order  $\Delta\omega_{\text{N}_2} < \Delta\omega_{\text{HCl}} < \Delta\omega_{\text{CO}}$ , which is roughly  
12 proportional to the polarity of the diatomic interacting with gas rare environment (i.e.  $\mu_{\text{N}_2} = 0$ ,  $\mu_{\text{CO}} =$   
13  $0.11 \text{ D}$  and  $\mu_{\text{HCl}} = 1.109$ , in Debye), although stronger for  $\text{CO}$ .  
14  
15  
16  
17  
18  
19  
20

## 21 VI. CONCLUSIONS

22 The present work attempts to assess and evaluate the performance of the corrected dispersion  
23 density functional method in describing  $\text{N}_2\text{-Ar}_n$  van der Waals complexes, which are characterized by  
24 the dominance of pure dispersion interactions. Hence, we show that dispersion-corrected DFT  
25 provides an accurate and reliable framework to investigate weak interactions between small molecules  
26 and noble gas atoms. We illustrate also the use of the Grimme's PBE-D3 approach which may provide  
27 a uniform formalism for the treatment of molecules in gas phase, adsorbed on surfaces or embedded in  
28 matrices, and in solid state. Our results reveal that there are slight changes on both geometrical  
29 parameters and vibrational frequency on  $\text{N}_2$  upon embedding on van der Waals matrices. We also  
30 demonstrate that these effects remain unchanged from cluster containing few Ar atoms up to full  
31 matrix embedding (up to 107 Ar atoms surrounding  $\text{N}_2$ ). These effects are rationalized in terms of the  
32 equivalence of bimolecular interaction potentials between  $\text{N}_2\text{-Ar}$  and  $\text{Ar-Ar}$  species.  
33  
34  
35  
36  
37  
38  
39

40 Using a periodic approach to matrix embedding, we show that we can model the  $\text{N}_2$  molecule  
41 and its interactions with a rare gas matrix. However, cautions should be taken when comparing  
42 spectroscopic data obtained using matrix embedding to measurements in the gas-phase or to  
43 theoretical data of individual molecules, since the influence on spectroscopic properties can be  
44 significant. This approach has been developed in our laboratories to treat embedding of  $\text{CO}$  molecule  
45 and it is currently being further developed for other neutral and charged molecules relevant for  
46 astrophysical, planetary or atmospheric media (e.g.  $\text{CN}$ ,  $\text{N}_2^+$ ,  $\text{CO}_2 \dots$ ).  
47  
48  
49  
50  
51

## 52 ACKNOWLEDGMENTS

53 We acknowledge the International Scientific Partnership Program ISPP at King Saud  
54 University for funding this research work through ISPP# 0045 and the Marie Curie International  
55 Research Staff Exchange Scheme Fellowship within the 7th European Community Framework  
56 Program under Grant No. IRSES- GA-2012-31754. We acknowledge the VIPER high-performance  
57  
58  
59  
60

1  
2  
3 computing facility of the University of Hull and its support team. The supports of the COST Actions  
4 CM1405 (MOLIM: MOLEcules In Motion) and CM1401 (Our Astro-Chemical History) are also  
5 acknowledged.  
6  
7  
8  
9  
10  
11  
12  
13  
14  
15  
16  
17  
18  
19  
20  
21  
22  
23  
24  
25  
26  
27  
28  
29  
30  
31  
32  
33  
34  
35  
36  
37  
38  
39  
40  
41  
42  
43  
44  
45  
46  
47  
48  
49  
50  
51  
52  
53  
54  
55  
56  
57  
58  
59  
60

**References**

- (1) Sauer, J.; Ugliengo, P.; Garrone, E.; Saunders, V. R. Theoretical Study of van der Waals Complexes at Surface Sites in Comparison with the Experiment. *Chem. Rev.* **1994**, *94*, 2095-2160.
- (2) Grimme, S. and Steinmetz, M. Effects of London dispersion correction in density functional theory on the structures of organic molecules in the gas phase. *Phys. Chem. Chem. Phys.* **2013**, *15*, 16031-16042.
- (3) Grimme, S. Density functional theory with London dispersion corrections. *Comput. Mol. Sci.* **2011**, *1*, 211–228.
- (4) Andrews, L. Spectroscopy of Molecular Ions in Noble Gas Matrices. *Ann. Rev. Phys. Chem.* **1979**, *30*, 79-101.
- (5) Chabbi, H.; Dahoo, P. R.; Lakhlifi, A. Spectroscopy of O<sub>3</sub> trapped in rare gas matrices. II. Vibrational energies and transition moments of low-lying levels. *J. Chem. Phys.* **1999**, *111*, 10202-10209.
- (6) Cahill, J. E.; Leroi, G. E. Raman Spectra of Solid CO<sub>2</sub>, N<sub>2</sub>O, N<sub>2</sub>, and CO. *J. Chem. Phys.* **1969**, *51*, 1324-1331.
- (7) Boursey, E.; Roncin, J. Y. Experimental Deperturbation of the  $b^1\Pi_u \leftarrow X^1\Sigma_g^+$  Transition of N<sub>2</sub> in the Solid State, Pure and Trapped in Ne and CF<sub>4</sub> Matrices at Low Temperature. *Phys. Rev. Lett.* **1971**, *26*, 308-311.
- (8) Fraenkel, R.; Haas, Y. Trapping of guests in a rare gas matrix: A molecular dynamics simulation. *J. Chem. Phys.* **1994**, *100*, 4324- 4328.
- (9) Busseron, E.; Ruff, Y.; Moulin E.; Giuseppone N. Supramolecular self-assemblies as functional nanomaterials. *Nanoscale*. **2013**, *5*, 7098-7140.
- (10) Dhotel, A.; Chen, Z.; Delbreilh, L.; Youssef, B.; Saiter, J-M.; Tan, L. Molecular Motions in Functional Self-Assembled Nanostructures. *Int. J. Mol. Sci.* **2013**, *14*, 2303-2333.
- (11) Becke, A. D. Density-functional thermochemistry. V. Systematic optimization of exchange-correlation functional. *J. Chem. Phys.* **1997**, *107*, 8554-8560.
- (12) Langreth, D. C.; Dion, M.; Rydberg, H.; Schröder, E.; Hyldgaard, P.; Lundqvist, B.I. Van der Waals density functional theory with applications. *Int. J. Quantum Chem.* **2005**, *101*, 599-610.
- (13) Jeziorski B.; Szalewicz, K. in: edited by von Rague-Schleyer P. *Encyclopedia of Computational Chemistry*; Wiley, New York, Vol. 2, **1998**, p.1376.
- (14) Jansen G.; Heßelmann, A. Comment on “Using Kohn–Sham Orbitals in Symmetry-Adapted Perturbation Theory To Investigate Intermolecular Interactions”. *J. Phys. Chem. A.* **2001**, *105*, 11156-11157.
- (15) Bludský, O.; Rubeš, M.; Soldán, P.; Nachtigall, P. Investigation of the benzene-dimer potential energy surface: DFT/CCSD(T) correction scheme. *J. Chem. Phys.* **2008**, *128*, 114102.
- (16) Dunning Jr., T.H. Gaussian basis sets for use in correlated molecular calculations. I. The atoms boron through neon and hydrogen. *J. Chem. Phys.* **1989**, *90*, 1007-1023.

- 1  
2  
3 (17) Grimme, S.; Antony, J.; Ehrlich, S.; Krieg, H. A consistent and accurate ab initio parametrization  
4 of density functional dispersion correction (DFT-D) for the 94 elements H-Pu. *J. chem. Phys.* **2010**,  
5 *132*, 154104.  
6  
7 (18) Grimme, S.; Hansen, A.; Brandenburg, J. G.; Bannwarth, C. Dispersion-Corrected Mean-Field  
8 Electronic Structure Methods. *Chem. Rev.* **2016**, *116*, 5105-5154.  
9  
10 (19) Grimme, S. Accurate description of van der Waals complexes by density functional theory  
11 including empirical corrections. *J. Comput. Chem.* **2004**, *25*, 1463-1473.  
12  
13 (20) Grimme, S. Semiempirical GGA-type density functional constructed with a long-range dispersion  
14 correction. *J. Comput. Chem.* **2006**, *27*, 1787-1799.  
15  
16 (21) Slanina, Z.; Kim, S. J.; Fox, K. Thermodynamics of Ar-N<sub>2</sub> Complexes and Their Abundance in  
17 Titan's Atmosphere. *Thermochimica Acta.* **1994**, *232*, 111-116.  
18  
19 (22) Crifo, J. F.; Slanina, Z.; Vigasin, A. *Molecular Complexes in Earth's Planetary, Cometary and*  
20 *Interstellar Atmospheres*. World Scientific Publishing, Singapore, 1998.  
21  
22 (23) Slanina, Z.; Kim, S. J.; Fox, K. Computational studies of atmospheric chemistry species. Part XI.  
23 A computational study of two Ar-N<sub>2</sub> complexes. *J. molec. Struct. Theochem* **1993**, *288*, 17-20.  
24  
25 (24) Zhu, J.; Lu, Y.-P.; Chen, X.-R.; Cheng, Y. Ab initio study for the intermolecular interaction  
26 potential surface of Ar-N<sub>2</sub> complex. *Eur. Phys. J. D.* **2005**, *33*, 43-48.  
27  
28 (25) Beneventi, L.; Casavecchia, P.; Volpi, G. G.; Wong, C. C. K.; McCourt, F. R. W. Multiproperty  
29 determination of a new N<sub>2</sub>-Ar intermolecular interaction potential energy surface. *J. Chem. Phys.*  
30 **1993**, *98*, 7926-7939.  
31  
32 (26) Wang, F.; McCourt, F. R. W.; Le Roy, R. J. Use of simulated infrared spectra to test N<sub>2</sub>-Ar pair  
33 potentials and dipole moment surfaces. *Mol. Phys.* **1996**, *88*, 821- 840.  
34  
35 (27) Wishnow, E. H.; Gush, H. P.; Ozier, I. Far-infrared spectrum of N<sub>2</sub> and N<sub>2</sub>-noble gas mixtures  
36 near 80 K. *J. Chem. Phys.* **1996**, *104*, 3511-3516.  
37  
38 (28) Naumkin, F.Y. Molecular versus atom-atom interaction anisotropy in the case of the Ar-N<sub>2</sub> van  
39 der Waals system. *Mol. Phys.* **1997**, *90*, 875-888.  
40  
41 (29) Fernandez, B.; Koch, H.; Makarewicz, J. Accurate intermolecular ground state potential of the  
42 Ar-N<sub>2</sub> complex. *J. Chem. Phys.* **1999**, *110*, 8525-8532.  
43  
44 (30) Wang, F.; McCourt, F. R. W.; Le Roy, R. Dipole moment surfaces and the mid- and far-IR  
45 spectra of N<sub>2</sub>Ar. *J. Chem. Phys.* **2000**, *113*, 98-106.  
46  
47 (31) Patel, K.; Butler, P. R.; Ellis, A. M.; Wheeler, M. D. Ab initio study of Rg-N<sub>2</sub> and Rg-C<sub>2</sub> van der  
48 Waals complexes (Rg=He, Ne, Ar). *J. Chem. Phys.* **2003**, *119*, 909-920.  
49  
50 (32) Munteanu, C. R.; Cacheiro, J. L.; Fernández, B. Accurate intermolecular ground state potential of  
51 the Ar-N<sub>2</sub> van der Waals complex. *J. Chem. Phys.* **2004**, *121*, 10419-10425.  
52  
53 (33) Dham, A. K.; McCourt, F. R. W.; Meath, W. J. Exchange-Coulomb Model Potential Energy  
54 Surface for the N<sub>2</sub>-Ar Interaction. *J. Chem. Phys.* **1995**, *103*, 8477-8491.  
55  
56  
57  
58  
59  
60

- 1  
2  
3 (34) Dham, A. K.; Meath, W. J.; Jechow, J. W.; McCourt, F. R. W. New exchange-Coulomb N<sub>2</sub>-Ar  
4 potential-energy surface and its comparison with other recent N<sub>2</sub>-Ar potential-energy surfaces. *J.*  
5 *Chem. Phys.*, **2006**, *124*, 034308-22.  
6  
7 (35) Fu, H.; Zheng R.; Zheng, L. Theoretical studies of three-dimensional potential energy surfaces  
8 using neural networks and rotational spectra of the Ar-N<sub>2</sub> complex. *Mol. Phys.* **2016**, *114*, 72-82.  
9  
10 (36) Henderson, G.; Ewing, G. E. Infra-red spectrum, structure and properties of the N<sub>2</sub>-Ar van der  
11 Waals molecule. *Mol. Phys.* **1974**, *27*, 903-915.  
12  
13 (37) McKellar, A.R.W. Infrared spectra of the (N<sub>2</sub>)<sub>2</sub> and N<sub>2</sub>-Ar van der Waals molecules. *J. Chem.*  
14 *Phys.* **1988**, *88*, 4190-4196.  
15  
16 (38) Jäger, W.; Gerry, M.C.L. The microwave spectrum of the van der Waals complex Ar-N<sub>2</sub>. *Chem.*  
17 *Phys. Lett.* **1992**, *196*, 274-279.  
18  
19 (39) Jäger, W.; Gerry, M. C. L.; Bissonnette, C.; McCourt, F. R.W. Pure rotational spectrum of, and  
20 potential-energy surface for, the Ar-N<sub>2</sub> Van der Waals complex. *Faraday Discuss.* **1994**, *97*, 105-118.  
21  
22 (40) Hewage, J. W.; Amar, F. G. Structural motifs and stability of small argon-nitrogen clusters. *J.*  
23 *Chem. Phys.* **2003**, *119*, 9021-9029.  
24  
25 (41) Hewage, J. W.; Amar, F. G.; de Feraudy, M.-F.; Torchet, G. The structure of mixed nitrogen-  
26 Argon clusters. *Eur. Phys. J. D.* **2003**, *24*, 249-252.  
27  
28 (42) Torchet, G.; de Feraudy, M.-F.; Loreaux, Y. Electron diffraction studies on mixed Ar+N<sub>2</sub> clusters.  
29 *J. Mol. Struct.* **1999**, *261*, 485-486.  
30  
31 (43) Fort, E.; Pradère, F.; De Martino, A.; Vach, H.; Châtelet, M. Diagnostics of mixed van der Waals  
32 clusters. *Eur. Phys. J. D.* **1998**, *1*, 79-84.  
33  
34 (44) Rühl, E.; Hitchcock, A. P.; Morin, P.; Lavollée, M. Core excitation in atomic and molecular  
35 clusters. *J. Chem. Phys.* **1995**, *92*, 521-540.  
36  
37 (45) Yang, S.; Philippe, L.; Châtelet, M. Formation and Characterization of Large (Ar)<sub>n</sub>, (N<sub>2</sub>)<sub>n</sub>, and  
38 Mixed (Ar)<sub>n</sub>(N<sub>2</sub>)<sub>m</sub> van der Waals Clusters Produced by Supersonic Expansion. *J. Clust. Sci.* **2007**, *18*,  
39 855-867.  
40  
41 (46) Nagasaka, M.; Serdaroglu, E.; Flesch, R.; Rühl, E.; Kosugi, N. Structures of mixed argon-  
42 nitrogen clusters. *J. Chem. Phys.* **2012**, *137*, 214305.  
43  
44 (47) Sanaa Zaag, A.; Yazidi, O.; Jaidane, N.-E.; Ross, M. W.; Castleman Jr., A. W.; Al-Mogren, M.  
45 M.; Linguetti R.; Hochlaf, M. Structure, Reactivity, and Fragmentation of Small Multi-Charged  
46 Methane Clusters. *J. Phys. Chem. A.* **2016**, *120*, 1669-1676.  
47  
48 (48) Elstner, M.; Hobza, P.; Frauenheim, T.; Suhai, S.; Kaxiras, E. Hydrogen bonding and stacking  
49 interactions of nucleic acid base pairs: A density-functional-theory based treatment. *J. Chem. Phys.*  
50 **2001**, *114*, 5149-5155.  
51  
52 (49) Jurečka, P.; Černý, J.; Hobza, P.; Salahub, D. R. Density functional theory augmented with an  
53 empirical dispersion term. Interaction energies and geometries of 80 noncovalent complexes compared  
54 with *ab initio* quantum mechanics calculations. *J. Comput. Chem.* **2007**, *28*, 555-569.  
55  
56  
57  
58  
59  
60

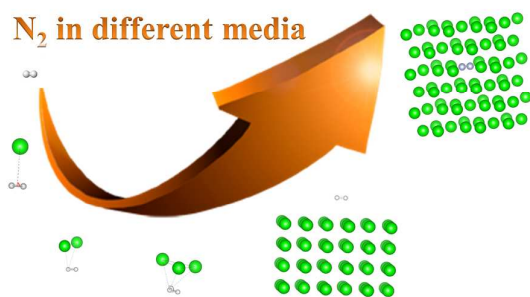
- 1  
2  
3 (50) Boussouf, K.; Boulmene, R.; Prakash, M.; Komaha, N.; Taleb, M.; Al-Mogren M. M.; Hochlaf,  
4 M. Characterization of  $Zn^{q+}$ -imidazole ( $q = 0, 1, 2$ ) organometallic complexes: DFT methods vs.  
5 standard and explicitly correlated post-Hartree-Fock methods. *Phys. Chem. Chem. Phys.* **2015**, *17*,  
6 14417-14426.  
7  
8 (51) Boulmene, R.; Boussouf, K.; Prakash, M.; Komaha, N.; Al-Mogren M. M.; Hochlaf, M. Ab Initio  
9 and DFT Studies on  $CO_2$  Interacting with  $Zn^{q+}$ -Imidazole ( $q=0, 1, 2$ ) Complexes: Prediction of Charge  
10 Transfer through  $\sigma$ - or  $\pi$ -Type Models. *Phys. Chem. Chem. Phys.* **2016**, *17*, 994-1005.  
11  
12 (52) Mahjoubi, K.; Benoit, D. M.; Jaidane, N.-E.; Al-Mogren M. M.; Hochlaf, M. Understanding of  
13 matrix embedding: a theoretical spectroscopic study of CO interacting with Ar clusters, surfaces and  
14 matrices. *Phys. Chem. Chem. Phys.* **2015**, *17*, 17159-17168.  
15  
16 (53) VandeVondele, J.; Hutter, J. Gaussian basis sets for accurate calculations on molecular systems in  
17 gas and condensed phases. *J. Chem. Phys.* **2007**, *127*, 114105.  
18  
19 (54) Naumkin, F. Y.; Knowles, P. J. On the adequacy of pairwise additive potentials for rare gas-  
20 halogen systems: The effect of anisotropy of interactions between atoms. *J. chem. Phys.* **1995**, *103*,  
21 3392-3399.  
22  
23 (55) Naumkin, F. Y.; Knowles, P. J.; *Femtochemistry - Ultrafast Chemical and Physical Processes in*  
24 *Molecular Systems*, edited by Chergui M. World Scientific :Singapore, **1996**, p.94.  
25  
26 (56) Goedecker, S.; Teter M.; Hutter, J. Separable dual-space Gaussian pseudopotentials. *Phys. Rev. B.*  
27 **1996**, *54*, 1703-1710.  
28  
29 (57) Lippert, G.; Hutter, J.; Parrinello, M. A hybrid Gaussian and plane wave density functional  
30 scheme. *Mol. Phys.* **1997**, *92*, 477-488.  
31  
32 (58) Krack, M.; Parrinello, M. in *High performance computing in chemistry, Report of the BMBF*  
33 *project, Grant Number 01IRA17 A-C*, edited by Grotendorst J.; FZ Jülich, Germany, **2004**, vol. 25 of  
34 NIC series.  
35  
36 (59) VandeVondele, J.; Krack, M.; Mohamed, F.; Parrinello, M.; Chassaing T.; Hutter, J. Quickstep:  
37 Fast and accurate density functional calculations using a mixed Gaussian and plane waves approach.  
38 *Computer Physics Communications.* **2005**, *167*, 103-128.  
39  
40 (60) Mundy, C. J.; Mohamed, F.; Schiffman, F.; Tabacchi, G.; Forbert, H.; Kuo, W.; Hutter, J.; Krack,  
41 M.; Iannuzzi, M.; McGrath, M. et al. CP2K software package, <http://cp2k.berlios.de>  
42  
43 (61) Krack, M. Pseudopotentials for H to Kr optimized for gradient-corrected exchange-correlation  
44 functional. *Theor. Chem. Acc.* **2005**, *114*, 145-152.  
45  
46 (62) Perdew, J. P.; Burke, K.; Ernzerhof, M. Generalized Gradient Approximation Made Simple. *Phys.*  
47 *Rev. Lett.* **1996**, *77*, 3865-3868.  
48  
49 (63) Byrd, R. H.; Lu, P.; Nocedal J.; Zhu, C. A Limited Memory Algorithm for Bound Constrained  
50 Optimization. *SIAM J. Sci. Comput.* **1995**, *16*, 1190-1208.  
51  
52 (64) Liu, B.; McLean, A. D. Accurate calculation of the attractive interaction of two ground state  
53 helium atoms. *J. Chem. Phys.* **1973**, *59*, 4557-4558.  
54  
55  
56  
57  
58  
59  
60

- 1  
2  
3 (65) Knowles, P. J.; Andrews, J. S.; Amos, R. D.; Handy, N. C.; Pople, J. A. Restricted Møller—  
4 Plesset theory for open-shell molecules. *Chem. Phys. Lett.* **1991**, *186*, 130-136.  
5  
6 (66) Møller C.; Plesset, M. S. Note on an Approximation Treatment for Many-Electron Systems. *Phys.*  
7 *Rev.* **1934**, *46*, 618-622.  
8  
9 (67) Curtiss, L. A.; Redfern, P. C.; Raghavachari, K.; Rassolov V.; Pople, J. A. Gaussian-3 theory  
10 using reduced Møller-Plesset order. *J. Chem. Phys.* **1999**, *110*, 4703-4709.  
11  
12 (68) Gaussian 09, Revision A.1, Frisch, M. J.; Trucks, G. W.; Schlegel, H. B.; Scuseria, G. E.; Robb,  
13 M. A.; Cheeseman, J. R.; Scalmani, G.; Barone, V.; Mennucci, B.; Petersson, G. A. et al. Gaussian,  
14 Inc., Wallingford CT, 2009.)  
15  
16 (69) **CFOUR, Coupled-Cluster techniques for Computational Chemistry**, a quantum-chemical  
17 program package by J.F. Stanton, J. Gauss, M.E. Harding, P.G. Szalay with contributions from A.A.  
18 Auer, R.J. Bartlett, U. Benedikt, C. Berger, D.E. Bernholdt, Y.J. Bomble, L. Cheng, O. Christiansen,  
19 F. Engel, R. Faber, M. Heckert, O. Heun, C. Huber, T.-C. Jagau, D. Jonsson, J. Jusélius, K. Klein,  
20 W.J. Lauderdale, F. Lipparini, D.A. Matthews, T. Metzroth, L.A. Mück, D.P. O'Neill, D.R. Price, E.  
21 Prochnow, C. Puzzarini, K. Ruud, F. Schiffmann, W. Schwalbach, C. Simmons, S. Stopkowicz, A.  
22 Tajti, J. Vázquez, F. Wang, J.D. Watts and the integral packages *MOLECULE* (J. Almlöf and P.R.  
23 Taylor), *PROPS* (P.R. Taylor), *ABACUS* (T. Helgaker, H.J. Aa. Jensen, P. Jørgensen, and J. Olsen),  
24 and ECP routines by A. V. Mitin and C. van Wüllen. For the current version, see <http://www.cfour.de>.  
25  
26 (70) Boys, S. F.; Bernardi, F. The calculation of small molecular interactions by the differences of  
27 separate total energies. Some procedures with reduced errors. *Mol. Phys.* **1970**, *19*, 553-566.  
28  
29 (71) K. P. Huber and G. Herzberg, *Molecular Spectra and Molecular Structure IV, Constants of*  
30 *diatomic Molecules* New York, Reinhold, 1979.  
31  
32 (72) Fujii, Y.; Lurie, N. A.; Pynn, R.; Shirane, G. Inelastic neutron scattering from solid <sup>36</sup>Ar. *Phys.*  
33 *Rev. B.* **1974**, *10*, 3647-3659.  
34  
35 (73) Halo, M.; Casassa, S.; Maschio, L.; Pisani, C. Local MP2 periodic study of rare-gas crystals.  
36 *Chem. Phys. Letters.* **2009**, *467*, 294–298.  
37  
38 (74) Prakash, M.; Mathivon, K.; Benoit, D. M.; Chambaud G.; Hochlaf, M. Carbon dioxide interaction  
39 with isolated imidazole or attached on gold clusters and surface: competition between  $\sigma$  H-bond and  $\pi$   
40 stacking interaction. *Phys. Chem. Chem. Phys.* **2014**, *16*, 12503–12509.  
41  
42 (75) Iori, F.; Corni S.; Di Felice, R. Unraveling the Interaction between Histidine Side Chain and the  
43 Au(111) Surface: A DFT Study. *J. Phys. Chem. C.* **2008**, *112*, 13540–13545.  
44  
45 (76) Lowen, H. W.; Jodl, H. J.; Loewenschuss A.; Daufer, H. Raman studies on N<sub>2</sub> – rare-gas mixed  
46 crystals. *Can. J. Phys.* **1988**, *66*, 308-315.  
47  
48 (77) Anderson, D. T.; Davis S.; Nesbitt, D. J. Sequential solvation of HCl in argon: High resolution  
49 infrared spectroscopy of Ar<sub>n</sub>HCl (n=1,2,3). *J. Chem. Phys.* **1997**, *107*, 1115-1127.  
50  
51  
52  
53  
54  
55  
56  
57  
58  
59  
60

1  
2  
3  
4  
5  
6  
7  
8  
9  
10  
11  
12  
13  
14  
15  
16  
17  
18  
19  
20  
21  
22  
23  
24  
25  
26  
27  
28  
29  
30  
31  
32  
33  
34  
35  
36  
37  
38  
39  
40  
41  
42  
43  
44  
45  
46  
47  
48  
49  
50  
51  
52  
53  
54  
55  
56  
57  
58  
59  
60



## Graphical Abstract

1  
2  
3  
4  
5  
6  
7  
8  
9  
10  
11  
12  
13  
14  
15  
16  
17  
18  
19  
20  
21  
22  
23  
24  
25  
26  
27  
28  
29  
30  
31  
32  
33  
34  
35  
36  
37  
38  
39  
40  
41  
42  
43  
44  
45  
46  
47  
48  
49  
50  
51  
52  
53  
54  
55  
56  
57  
58  
59  
60